Top-Down Feedback Controls Spatial Summation and Response Gain In Primate Visual Cortex

Lauri Nurminen[1]ǂ, Sam Merlin[1]ǂ, Maryam Bijanzadeh[1,2], Frederick Federer[1] and Alessandra Angelucci[1]*

[1] *Department of Ophthalmology and Visual Science, Moran Eye Institute*
AND
[2] *Interdepartmental Program in Neuroscience*
65 Mario Capecchi Drive
University of Utah, Salt Lake City, UT 84132, USA

ǂ These authors contributed equally to this work.

* Corresponding author (alessandra.angelucci@hsc.utah.edu)

In the cerebral cortex, sensory information travels along feedforward connections through a hierarchy of areas processing increasingly complex stimulus features[1]. Hierarchical processing, based solely on feedforward connections, has dominated most theories of sensory processing in neuroscience and computer vision over the past 50 years[2,3]. These theories, however, have disregarded the existence of anatomically more prominent feedback connections from higher- to lower-order cortical areas[1], whose function remains hypothetical. Feedback has been implicated in attention[4,5], expectation[6], and sensory context[7,8], but the cellular mechanisms underlying these diverse feedback functions are unknown. Moreover, it is controversial whether feedback modulates response gain[9-12] or surround suppression[13-15] (the modulatory influence of sensory context on neuronal responses[16-19]) in lower-order areas. Here we have performed the first specific inactivation of cortical feedback at millisecond-time resolution, by optogenetically inactivating feedback connections from the secondary (V2) to the primary visual cortex (V1) in primates. Moderate reduction of V2 feedback activity increased RF size and reduced surround suppression in V1, while strongly reducing feedback activity decreased response gain. Our study has identified a small set of fundamental operations as the cellular-level mechanisms of feedback-mediated top down modulations of early sensory processing. These operations allow the visual system to dynamically regulate spatial resolution, by changing RF size, its sensitivity to image features, by changing response gain, and efficiency of coding natural images, by providing surround suppression.

To determine the cellular mechanisms underlying the influence of cortical feedback on sensory processing, we asked whether inactivating feedback alters spatial summation and surround suppression in V1. Spatial summation is the property of V1 neurons to respond maximally to small stimuli in their RF, but reduce their response to larger stimuli extending into the RF surround[20-22]. Surround suppression is a basic computation in visual processing[7,16,17,19,23] thought to increase the neurons' efficiency of coding natural images[24-27], and to be generated by feedback connections[7,8,28]. However, the role of feedback in surround suppression has remained controversial. Inactivation of higher-order cortices has produced weak reduction in surround suppression in some studies[13-15], but only reduction in response gain in other studies[9-12]. These inactivation methods suppress activity in an entire cortical area, thus the observed effects could have resulted from indirect pathways through the thalamus or other cortical areas. Moreover, they do not allow fine control of inactivation levels, thus precluding potentially more physiologically relevant manipulations, and leaving open the possibility that the discrepant results simply reflected different levels of inactivation. To overcome the technical limitations of previous studies, we have used selective optogenetic inactivation of V2-to-V1 feedback terminals, while measuring spatial summation and surround suppression in V1 neurons using linear electrode arrays (**Fig.1a**).

To express the outward proton pump Archaerhodopsin-T (ArchT)[29] in the axon terminals of V2 feedback neurons, we injected into V2 of marmoset monkeys a mixture of Cre-expressing (AAV9.CaMKII.Cre) and Cre-dependent adeno-associated virus (AAV9) carrying the genes for ArchT and green fluorescent protein (AAV9.Flex.CAG.ArchT-GFP; see Methods). Intrinsic signal optical imaging was performed through thinned skull to identify the V1/V2 border

(**Fig.1b**), so as to restrict injections to V2 (**Fig.1c**). This viral vector combination produced selective anterograde infection of neurons at the injected site and virtually no retrograde infection of neurons in V1 (**Fig.1c,d**). About 2 months post-injection, linear array recordings were targeted to GFP/ArchT-expressing V1 regions, identified using GFP-goggles (**Fig.1d**). Spatial-summation curves of V1 neurons were measured using drifting sinusoidal gratings of increasing diameter in sufentanil-anesthetized and paralyzed marmosets. Trial interleaved and balanced surface laser stimulation of increasing intensity was applied to ArchT-expressing axon terminals of V2 feedback neurons, at the V1 recording site (see Methods). This approach allowed for selective inactivation of V2 feedback terminals in the superficial (but not deep) layers of V1.

We measured spatial summation curves of parafoveal V1 neurons using grating patches of increasing diameter centered on the neurons' RF. Typical V1 cells increase their response with stimulus diameter up to a peak (the RF size), and are suppressed for further increases in stimulus size (surround suppression) (**Fig.2a**). We present spatial summation measurements from 66 visually responsive and stimulus modulated, spike-sorted single units from 3 animals injected with AAVs. Approximately 61% (40/66) of single units were significantly modulated by the laser (see Methods). As laser-induced heat can alter cortical spiking activity[30], we selected a safe range of laser intensities (9-43 mW/mm^2), based on results from control experiments in cortex not expressing ArchT (see **Extended Data Figs.1-2** and Supplementary Information).

At low laser intensities (mean±sem 28.7±1.95mW/mm^2), the majority (76%) of laser-modulated units showed a shift of the spatial summation peak towards larger stimuli, i.e. an increase in RF size, which in 46% of cells was accompanied by an increase in the height of the peak, while in the remainder of cells RF size was unchanged (15%) or decreased (9%) (**Fig.2a-b**). Mean RF diameter was significantly smaller with intact feedback, compared to when feedback was inactivated, for cells showing increases in RF size (mean±s.e.m no-laser vs. laser: 1.12±0.08º vs. 1.93±0.08º, p<0.001; **Fig.2b$_1$**), cells showing both increases in RF size and peak response (1.14±0.08º vs. 2.04±0.20º, p<0.001; **Fig. 2b$_2$**), and even across the entire neuronal population (1.27±0.10º vs. 1.83±0.14º, p<0.01), with a mean increase of 56.2±10.7% (p<0.001; **Fig.2b$_3$**). Feedback inactivation increased mean RF diameter in all layers (**Fig.2b$_4$**) (no-laser vs. laser: supragranular layers 1.23±0.11º vs. 1.53±0.10º; granular layer 1.31±0.17º vs. 2.26±0.35°; infragranular layers 1.29±0.25º vs. 1.88±0.26º; p<0.05). In contrast, surround diameter was not affected by feedback inactivation across the population (p=0.33) or in individual layers (p>0.27) (see Supplementary Information).

As a result of increased RF size, caused by feedback inactivation, stimuli extending into the proximal surround (i.e. the surround region closest to the RF; see legend for quantitative definition), evoked larger neuronal responses (no-laser vs. laser: 36.4±12.3 vs. 43.5±17.2 spikes/s; mean increase 29.2±7.14%, p<0.001; **Fig.2c$_1$**), and, therefore, less surround suppression (or even facilitation) with feedback inactivated when compared with intact feedback. Laser stimulation reduced the suppression index (SI) for stimuli covering the RF and proximal surround, measured relative to the peak response in the no-laser condition (SI no-laser vs. laser: 0.21±0.03 vs. 0.006±0.0567, p<0.01; **Fig.2c$_2$**) (see Methods). In contrast, the response (no-laser vs. laser: 20.9±8.71 vs. 19.79 ±7.69 spikes/s; mean spike-rate increase 7.10±13.4%, p=0.92) and SI (no-laser vs. laser: 0.58±0.05 vs. 0.58±0.05; p=0.945; **Fig.2c$_3$**) evoked by stimuli extending into the more distal surround were unchanged by feedback inactivation. V2 feedback inactivation

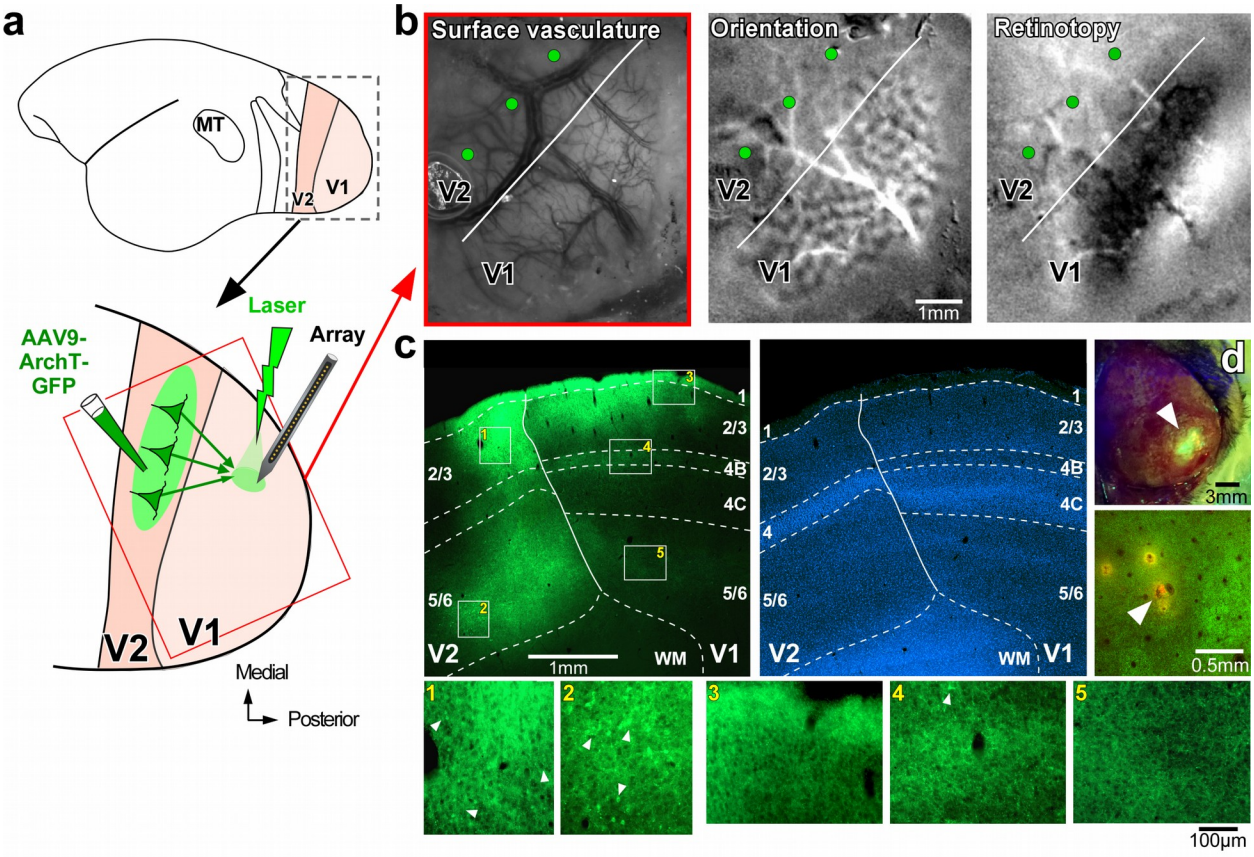

Figure 1

Figure 1. Viral injections and ArchT-GFP expression in feedback terminals. (a) TOP: Schematic of lateral view of the marmoset brain. Areas V1 and V2 inside the *boxed* region are shown enlarged at the bottom. BOTTOM: Schematics of the inactivation paradigm: viral injections were targeted to V2, array recordings and photoactivation to V1. *Red box*: approximate location of the imaged region in (b). **(b)** Orientation-preference and retinotopy maps, imaged under red light, were used to identify the V1/V2 border (*white line*), and to target multiple viral injections (*green dots*) to V2, using as reference the surface vasculature, imaged under green light. **(c) TOP** LEFT: Sagittal section through V1 and V2, viewed under GFP fluorescence, showing two viral injection sites confined to V2, and resulting expression of ArchT-GFP in the axon terminals of V2 feedback neurons within V1 layers 1-3, 4B and 5/6 (typical feedback laminar termination pattern[39,40]). This section was located near the lateralmost aspect of the hemisphere, therefore the infragranular layers are elongated due to the lateral folding-over of the cortical sheet. *Solid contour*: V1/V2 border. *Dashed contours:* laminar borders delineated on the same section counterstained with DAPI (TOP RIGHT). BOTTOM *(panels 1-5):* higher magnification of label inside the *white boxes numbered 1-5* in the top-left panel. Panels 1-2 show clusters of labeled somata (*arrowheads*) at the V2 injection sites; instead there is only one labeled soma (*arrowhead*) in panel 4, and none in panels 3,5. **(d)** TOP: GFP excitation (*arrowhead*) through the intact thinned skull, approximately two months after injection. BOTTOM: Tangential section through V1 showing the location of a DiI-coated electrode penetration (*arrowhead*) amid ArchT-GFP-expressing feedback axon terminals (*green fluorescence*).

is, indeed, expected to affect most strongly the suppression arising from the proximal surround, and to not abolish distal surround suppression. This is because feedback connections from V2 do not extend into the distal surround of V1 neurons, unlike feedback connections from areas V3 and MT[28], which were unperturbed in this study.

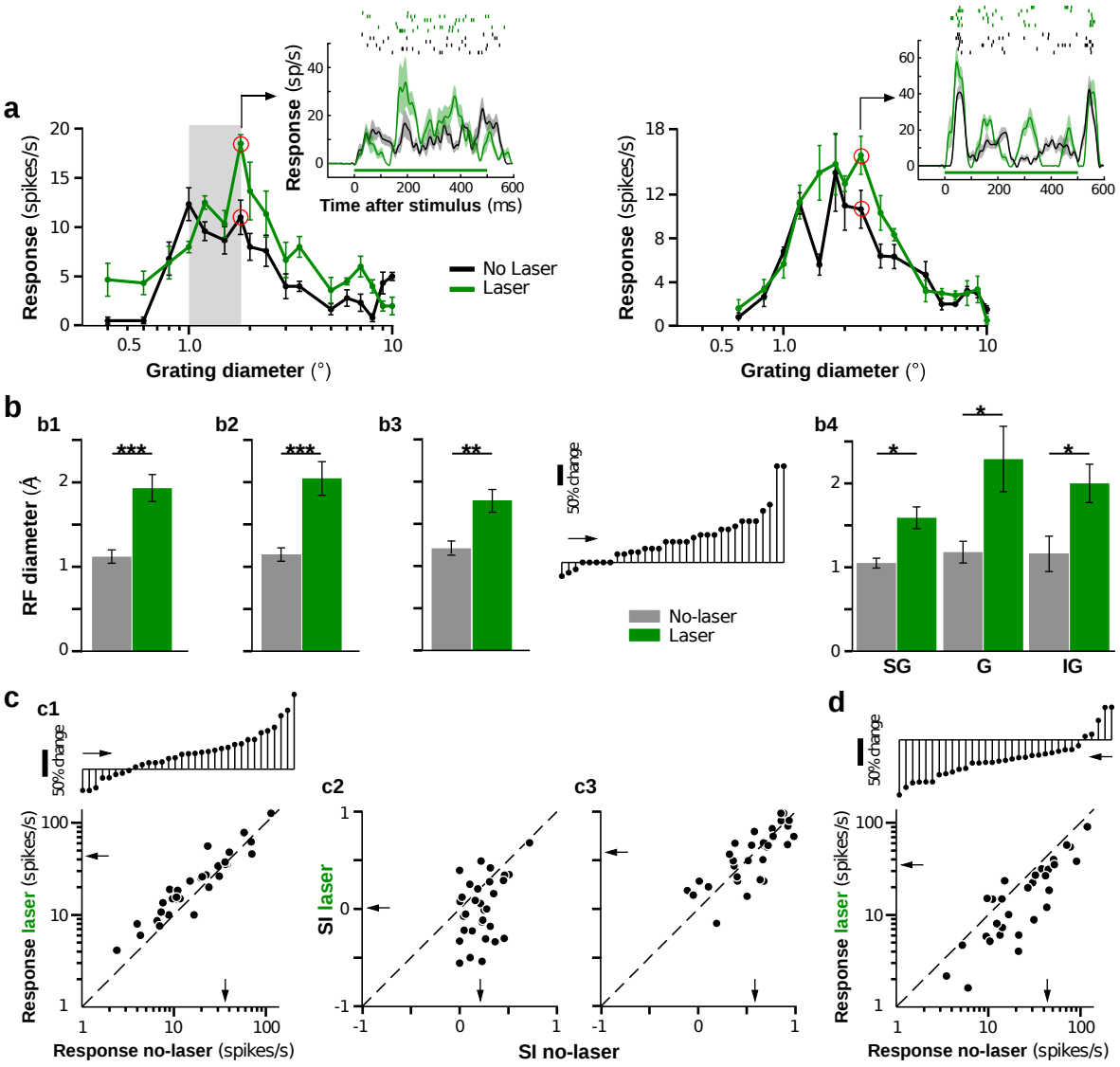

Figure 2

Figure 2. Feedback controls RF size and surround suppression. (a) Spatial summation curves for two example V1 cells recorded with (*green*) and without (*black*) laser stimulation. *Gray area in left panel:* proximal surround. *Insets:* PSTHs (bottom) and raster plots (top) measured at the stimulus diameters indicated by *red circles* in the respective size tuning curves. **(b)** Mean RF size (diameter at peak response) with and without laser stimulation for: **(b_1)** cells showing increased RF size with laser stimulation (n=25), **(b_2)** cells showing both increased RF size and peak response (n=12), and **(b_3)** LEFT: all cells (n=33); RIGHT: Cell-by-cell percent change in RF size across the entire cell population. *Arrow*: mean. **(b_4)** Mean RF size for the same population as in (b_3), but grouped according to layer. **(c)** Changes in surround-suppression with V2-feedback inactivated. **(c_1)** BOTTOM: response with and without laser for stimuli involving the RF and proximal surround (the latter defined as the stimulus diameter at the peak of the green spatial-summation curve). TOP: Cell-by-cell percent response change caused by laser stimulation, for stimuli extending into the proximal surround. Downward and upward stem: decreased and increased response, respectively. Scale bar: 50% change in response. **(c_2)** SI with and without laser for stimuli extending into the proximal surround. A SI of 1 indicates maximal suppression, a SI of 0 indicates no suppression, and negative SI

values indicate facilitation (see Methods). **(c_3)** Same as (c_2) but for stimuli extending into the distal surround (largest stimulus used). **(d)** BOTTOM: response with and without laser for stimuli confined to the RF (defined as the stimulus diameter at the peak of the black spatial-summation curve). TOP: Cell-by-cell percent response change caused by laser stimulation for stimuli confined to the RF.

Consistent with previous studies of V2 inactivation[10,12], we also found that stimuli confined to the neurons' RF (i.e. the spatial summation peak in the no-laser condition) evoked lower responses in the laser condition (35.1±15.3 spikes/s) vs. the non-laser condition (43.8±14.1; mean reduction 32.0±6.03%, $p<10^{-5}$; **Fig.2d**). There was a moderate, but statistically insignificant, relationship between response reduction to stimuli in the RF and change in RF diameter when feedback was inactivated (r=-0.31, p=0.11, Pearson's correlation), as well as between change in RF diameter and release from suppression in the proximal surround (r=0.32, p=0.08).

Prolonged light pulses directed on ArchT-expressing axon terminals have been shown to facilitate synaptic transmission, while ArchT photoactivation is consistently suppressive for pulse widths of ≤ 200ms[31]. Thus, we performed the analysis described above focusing only on the first 200ms of the response. The results of the original and shorter time-scale analyses were qualitatively and quantitatively similar (see Supplementary Information).

There is a controversy among previous studies over whether feedback inactivation causes general reduction of neuronal responses to small and large stimuli or reduced surround suppression in V1[9-15]. We found that general response reduction occurs for higher levels of feedback inactivation. About 36% of neurons that showed reduced surround suppression and/or increased RF size at low laser intensities, showed overall reduced response at higher laser intensities (mean±sem 36.1±1.52 mW/mm^2) (**Fig.3a**). Notably, at the laser intensity producing the largest general suppression, the RF diameter was still significantly smaller with intact feedback (1.19±0.11º) compared to when feedback was inactivated (1.60±0.14º, p<0.05; **Fig.3b**), but surround diameter was not significantly affected (p=0.57; see Supplementary Information). High-intensity laser stimulation significantly reduced responses to stimuli of any size, i.e. those confined to the RF (no-laser vs. laser: 53.1±9.26 vs. 21.8±3.01 spikes/s; mean reduction: 54.4±3.99%, $p<10^{-7}$; **Fig.3c**), as well as stimuli extending into the proximal surround (no-laser vs. laser*:* 43.1±9.07 vs. 26.5±4.12 spike/s; mean reduction: 28.3±6.14%, p<0.001; **Fig.3d**), or into the distal surround (no-laser vs. laser: 13.3±3.27 vs. 7.12±1.38 spike/s; mean reduction: 33.2±8.27%, p<0.01; **Fig.3e**). There were no statistically significant differences in spike-width, maximum spike-rate, baseline, or trial-by-trial variability between cells showing general suppression at higher laser intensity and cells that did not. However, the former had stronger surround suppression in the no-laser condition (SI: 0.78±0.03.1% vs. 0.49±0.07%, p<0.05), and were most prevalent in supragranular layers (albeit this was not statistically significant, $p_{bootstrap}$=0.06; **Fig.3f**). As the effective irradiance is higher in supragranular than in other layers, it is likely that a larger proportion of cells in the infragranular layers would have shown general suppression, had higher irradiance been delivered to the deeper layers.

Our study elucidates the cellular-level basis of how feedback affects information processing in the primate early visual cortex. Depending on its level of activity, feedback from V2 controls RF size, surround suppression, and the overall gain of neuronal responses in V1. Changes in RF size can dynamically alter the visual system's spatial resolution; increasing surround suppression provides efficient coding of natural images; increasing response gain improves sensitivity to

image features.

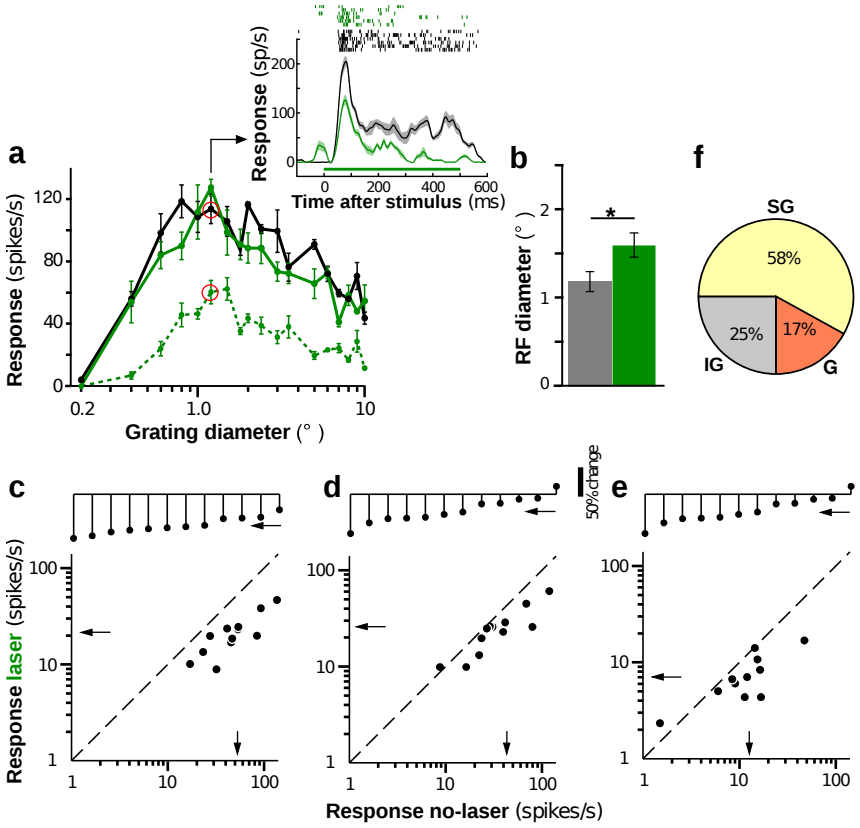

Figure 3

Figure 3. Feedback controls the overall gain of V1 responses. (a) Spatial-summation curve for one example V1 cell measured without laser (*black*) and with laser stimulation at two different intensities (*solid green*: 9mW/mm^2; *dashed green:* 43mW/mm^2). Other conventions as in **Fig. 2a**. **(b)** Mean RF diameter with and without laser for the population of cells showing general suppression (n=12). **(c)** BOTTOM: response with and without laser, and TOP: Cell-by-cell percent response reduction caused by laser stimulation, for stimuli confined to the RF. **(d-e)** Same as (c) but for stimuli covering the RF and proximal surround (d) or the full extent of the surround (e). **(f)** Distribution of cells showing general suppression across V1 layers.

Several forms of top-down influences in sensory processing have been shown to affect neuronal responses in the same way as we have shown, here, for feedback from V2. For example, spatial attention, one of the most studied instances of top-down modulation, increases the response gain of neurons at attended locations[4,32], modulates surround suppression[33,34], and, at least in parafoveal V1, reduces RF size[35]. Our results suggest that these effects of spatial attention are mediated by top-down modulations of feedback to early visual areas.

Previous inactivation studies have disagreed over whether feedback regulates surround suppression or the overall gain of V1 neuron responses[9-15]. Our study resolves this controversy, and suggests that this discrepancy can, in fact, be attributed to different levels of feedback inactivation achieved in different studies.

Consistent with our findings, a role for feedback in spatial summation and surround suppression is predicted by recurrent network models of V1, in which the local network becomes more dominated by inhibition with increasing excitatory input drive[36-38]. In these models, reducing excitatory feedback inputs to the V1 cells' RF, and thus to the local network, weakens inhibition, allowing neurons to summate excitatory signals over larger visual field regions (i.e. to increase their RF size), until inhibition increases again, leading to surround suppression.

In summary, our study points to a crucial role of feedback in early visual processing, and identifies a small set of fundamental operations, changes in RF size, gain and surround suppression, as the cellular-level mechanisms of feedback-mediated top-down modulations of sensory responses.

REFERENCES

1 Van Essen, D. C. & Maunsell, J. H. R. Hierarchical organization and functional streams in the visual cortex. *Trends Neurosci.* **6**, 370-375 (1983).

2 Riesenhuber, M. & Poggio, T. in *The Visual Neurosciences* Vol. 2 (eds L. M. Chalupa & J. S. Werner) (MIT Press, 2003).

3 Hubel, D. H. & Wiesel, T. N. Receptive fields, binocular interaction and functional architecture in the cat's visual cortex. *J. Physiol. (Lond.)* **160**, 106-154. (1962).

4 McAdams, C. J. & Reid, C. R. Attention modulates the responses of simple cells in monkey primary visual cortex. *J. Neurosci.* **25**, 11023-11033 (2005).

5 Luck, S. J., Chelazzi, L., Hillyard, S. A. & Desimone, R. Neural mechanims of spatial selective attention in areas V1, V2 and V4 of macaque visual cortex. *J. Neurophysiol.* **77**, 24-42 (1997).

6 Rao, R. P. & Ballard, D. H. Predictive coding in the visual cortex: a functional interpretation of some extra-classical receptive-field effects. *Nat. Neurosci.* **2**, 79-87 (1999).

7 Angelucci, A. *et al.* Circuits and mechanisms for surround modulation in visual cortex. *Ann. Rev. Neurosci.* **40**, In Press (2017).

8 Angelucci, A. & Bressloff, P. C. The contribution of feedforward, lateral and feedback connections to the classical receptive field center and extra-classical receptive field surround of primate V1 neurons. *Prog. Brain Res.* **154**, 93-121 (2006).

9 Zhang, S. *et al.* Selective attention. Long-range and local circuits for top-down modulation of visual cortex processing. *Science* **345**, 660-665 (2014).

10 Hupé, J. M., James, A. C., Girard, P. & Bullier, J. Response modulations by static texture surround in area V1 of the macaque monkey do not depend on feedback connections from V2. *J. Neurophysiol.* **85**, 146-163. (2001).

11 Wang, C., Huang, J. Y., Bardy, C., FitzGibbon, T. & Dreher, B. Influence of 'feedback' signals on spatial integration in receptive fields of cat area 17 neurons. *Brain Res.* **1328**, 34-48 (2010).

12 Sandell, J. H. & Schiller, P. H. Effect of cooling area 18 on striate cortex cells in the squirrel monkey. *J. Neurophysiol.* **48**, 38-48. (1982).

13 Hupé, J. M. *et al.* Cortical feedback improves discrimination between figure and background by V1, V2 and V3 neurons. *Nature* **394**, 784-787. (1998).

14 Bardy, C., Huang, J. Y., Wang, C., Fitzgibbon, T. & Dreher, B. "Top-down" influences of ispilateral or contralateral postero-temporal visual cortices on the extra-classical receptive fields of neurons in cat's striate cortex. *Neurosci.* **158**, 951-968 (2009).

15 Nassi, J. J., Lomber, S. G. & Born, R. T. Corticocortical feedback contributes to surround suppression in V1 of the alert primate. *J. Neurosci.* **33**, 8504-8517 (2013).

16 Hubel, D. H. & Wiesel, T. N. Receptive fields and functional architecture in two nonstriate visual areas (18 and 19) of the cat. *J. Neurophysiol.* **28**, 229-289 (1965).

17 Allman, J., Miezin, F. & Mc Guinness, E. Stimulus specific responses from beyond the classical receptive field: Neurophysiological mechanisms for local-global comparisons in visual neurons. *Ann. Rev. Neurosci.* **8**, 407-430 (1985).

18 Angelucci, A. & Shushruth, S. in *The new visual neurosciences* (eds L. M. Chalupa & J. S. Werner) Ch. 30, 425-444 (MIT press, 2013).

19 Van den Bergh, G., Zhang, B., Arckens, L. & Chino, Y. M. Receptive-field properties of V1 and V2 neurons in mice and macaque monkeys. *J. Comp. Neurol.* **518**, 2051-2070 (2010).

20 Shushruth, S., Ichida, J. M., Levitt, J. B. & Angelucci, A. Comparison of spatial summation properties of neurons in macaque V1 and V2. *J. Neurophysiol.* **102**, 2069-2083 (2009).

21 Cavanaugh, J. R., Bair, W. & Movshon, J. A. Nature and interaction of signals from the receptive field center and surround in macaque V1 neurons. *J. Neurophysiol.* **88**, 2530-2546. (2002).

22 Sceniak, M. P., Hawken, M. J. & Shapley, R. M. Visual spatial characterization of macaque V1 neurons. *J. Neurophysiol.* **85**, 1873-1887 (2001).

23 Nurminen, L., Kilpelainen, M., Laurinen, P. & Vanni, S. Area summation in human visual system: psychophysics, fMRI, and modeling. *J. Neurophysiol.* **102**, 2900-2909 (2009).

24 Olshausen, B. A. & Field, D. J. Emergence of simple-cell receptive field properties by learning a sparse code for natural images. *Nature* **381**, 607-609 (1996).

25 Schwartz, O. & Simoncelli, E. P. Natural signal statistics and sensory gain control. *Nat. Neurosci.* **4**, 819-825 (2001).

26 Vinje, W. E. & Gallant, J. L. Natural stimulation of the nonclassical receptive field increase information transmission efficiency in V1. *J. Neurosci.* **22**, 2904-2915 (2002).

27 Nurminen, L. & Angelucci, A. Multiple components of surround modulation in primary visual cortex: multiple neural circuits with multiple functions? *Vision Res.* **104**, 47-56 (2014).

28 Angelucci, A. *et al.* Circuits for local and global signal integration in primary visual cortex. *J. Neurosci.* **22**, 8633-8646 (2002).

29 Han, X. *et al.* A high-light sensitivity optical neural silencer: development and application to optogenetic control of non-human primate cortex. *Front. Syst. Neurosci.* **5**, 18 (2011).

30 Stujenske, J. M., Spellman, T. & Gordon, J. A. Modeling the Spatiotemporal Dynamics of Light and Heat Propagation for In Vivo Optogenetics. *Cell Rep.* **12**, 525-534 (2015).

31 Mahn, M., Prigge, M., Ron, S., Levy, R. & Yizhar, O. Biophysical constraints of optogenetic inhibition at presynaptic terminals. *Nat Neurosci* **19**, 554-556 (2016).

32 McAdams, C. J. & Maunsell, J. H. Effects of attention on orientation-tuning functions of single neurons in macaque cortical area V4. *J. Neurosci.* **19**, 431-441 (1999).

33 Ito, M. & Gilbert, C. D. Attention modulates contextual influences in the primary visual cortex of alert monkeys. *Neuron* **22**, 593-604 (1999).

34 Sundberg, K. A., Mitchell, J. F. & Reynolds, J. H. Spatial attention modulates center-surround interactions in macaque visual area v4. *Neuron* **61**, 952-963 (2009).

35 Roberts, M. J., Delicato, L. S., Herrero, J., Gieselmann, M. A. & Thiele, A. Attention alters spatial integration in macaque V1 in an eccentricity dependent manner. *Nat. Neurosci.* **10**, 1483-1491 (2007).

36 Schwabe, L., Obermayer, K., Angelucci, A. & Bressloff, P. C. The role of feedback in shaping the extra-classical receptive field of cortical neurons: a recurrent network model. *J. Neurosci.* **26**, 9117-9129 (2006).

37 Shushruth, S. *et al.* Strong recurrent networks compute the orientation-tuning of surround modulation in primate primary visual cortex. *J. Neurosci.* **4**, 308-321. (2012).

38 Rubin, D. B., Van Hooser, S. D. & Miller, K. D. The stabilized supralinear network: a unifying circuit motif underlying multi-input integration in sensory cortex. *Neuron* **85**, 402-417 (2015).

39 Rockland, K. S. in *Primary Visual Cortex in Primates* Vol. 10 *Cerebral Cortex* (eds A. Peters & K. S. Rockland) 261-299 (Plenum Press, 1994).

40 Federer, F., Merlin, S. & Angelucci, A. Anatomical and functional specificity of V2-to-V1 feedback circuits in the primate visual cortex. *Soc. Neurosci. Abstr. Online.*, 699.602. (2015).

Acknowledgments. We thank Kesi Sainsbury for technical assistance. This work was supported by grants from the National Institute of Health (R01 EY026812, R01 EY019743, BRAIN U01 NS099702), the National Science Foundation (IOS 1355075, EAGER 1649923), the University of Utah Research Foundation, The University of Utah Neuroscience Initiative, to A.A., a grant from Research to Prevent Blindness, Inc. to the Department of Ophthalmology, University of Utah, and a postdoctoral fellowship from the Ella and Georg Ehrnrooth Foundation to L.N.

Author contributions L.N., S.M., M.B. and A.A. designed project and collected electrophysiological data. L.N, S.M. and F.F. performed optical imaging and viral injections. L.N. analyzed optogenetic and electrophysiological data. S.M. analyzed optical imaging data and histological expression of GFP label. S.M. and F.F. generated histological figures. L.N. and S.M. built the optogenetic stimulation system. A.A. supervised all aspects of project. L.N., S.M. and A.A. wrote the paper. All authors discussed the results, commented on and approved the final manuscript.

Author Information The authors declare no competing financial interests. Correspondence should be addressed to A.A. (alessandra.angelucci@hsc.utah.edu).

METHODS

Surgery and Viral Injections

All procedures conformed to the guidelines of the University of Utah Institutional Animal Care and Use Committee. Each of three marmoset monkeys (*Callithrix jacchus*) received 2-3 injections in dorsal area V2 of a 1:1 viral mixture of AAV9.CaMKII.Cre ($3.7x10^{13}$ particles/ml) and AAV9.Flex.CAG.ArchT-GFP ($9.8x10^{12}$ particles/ml; Penn Vector Core, University of Pennsylvania, PA). Injections were targeted and confined to V2 using as guidance the location of the V1/V2 border identified *in vivo* using intrinsic signal optical imaging. Surgical procedures were as previously described[41]. Briefly, animals were pre-anesthetized with ketamine (25-30mg/kg, i.m.) and xylazine (1mg/kg, i.m.), intubated, artificially ventilated with N_2O and O_2 (70:30), and the head was stereotaxically positioned. Anesthesia was maintained with isoflurane (1-2%), and end-tidal CO_2, SPO_2, electrocardiogram, and body temperature were monitored continuously. The scalp was opened and the skull was thinned using a dental drill over areas V1/V2, covered with agar and a coverslip, which was glued to the skull. On completion of surgery, isofluorane was turned off, anesthesia maintained with sufentanil citrate (8-13µg/kg/hr, i.v.), and paralysis was induced with repeated 30-60 min intravenous boluses of rocuronium bromide (0.6mg/kg/hr) to stabilize the eyes. The pupils were dilated with a topical short-acting mydriatic agent (tropicamide), the corneas protected with gas-permeable contact lenses, the eyes were refracted, and optical imaging was started. Once the V1/V2 border was functionally identified, the glass coverslip was removed, small craniotomies and durotomies were performed over V2, and the viral mixture slowly pressure-injected (240nl/site at 500µm and again at 1200µm depth, using glass pipettes of 40-50µm tip diameter, 15 minutes/240nl). The thinned skull was reinforced with dental cement, the skin sutured and the animal recovered.

Optical Imaging

Acquisition of intrinsic signals was performed using the Imager 3001 (Optical Imaging Ltd, Israel) under red light illumination (630 nm). Imaging for orientation and retinotopy allows identification of the V1/V2 border (**Fig. 1b**). Orientation maps were obtained using full-field, high-contrast (100%), pseudorandomized achromatic drifting square-wave gratings of 8 orientations at 0.5-2.0 cycles/° spatial frequency and 2.85 cycles/s temporal frequency, moving back and forth, orthogonal to the grating orientation. Responses to same orientations were averaged across trials, baseline subtracted, and difference images obtained by subtracting the response to two orthogonal oriented pairs. V2 could be identified by larger orientation domains compared to V1 (**Fig. 1b**). Retinotopic maps were obtained by subtracting responses to monocularly presented oriented gratings occupying complementary adjacent strips of visual space, i.e. masked by 0.5-1° strips of gray repeating every 1-2°, with the masks reversing in position in alternate trials. The V1/V2 border was identified by the presence of retinotopic stripes in V1, as compared to their absence in V2 (**Fig. 1b**). In each case, reference images of the surface vasculature were taken under 546 nm illumination (green light), and later used as reference to position pipettes for viral vector injection.

Electrophysiological Recordings and Visual Stimulation

Following 62-68 days transport, after the vector injection, animals were anesthetized and paralyzed by continuous infusion of sufentanil citrate (6-13µg/kg/h) and vecuronium bromide

(0.3mg/kg/h), respectively, and vital signs were continuously monitored, as described above. The pupils were dilated with topical atropine, protected with lenses and refracted. GFP-expressing V2 injection sites and V1 axonal fields were identified with GFP goggles (**Fig.1d**), and small craniotomies were made over V1. Extra-cellular recordings were made in V1 with 24-channel linear multielectrode arrays (V-Probe, Plexon, Dallas, TX; 100µm contact spacing, 20µm contact diameter) coated in DiI (Molecular Probes, Eugene, OR) to assist with post-mortem reconstruction of the electrode penetrations, and lowered normal to the cortical surface to a 2-2.2 mm depth over 60-90min. A 128-channel system (Cerebus, Blackrock Microsystems, Salt Lake City, UT) was used for signal amplification and digitization (30 kHz). Continuous voltage traces were band-pass filtered (0.5-14.25 kHz), and spikes were detected as spatiotemporal waveforms using the double-threshold flood fill algorithm[42] (thresholds 2 and 4 x noise S.D.). This procedure was adopted because the apical dendrites of pyramidal cells run parallel to the probe shank and may spread the waveforms across multiple channels. A masked EM algorithm[43] was used for clustering, and manual refinement of the clusters was performed with the Klustasuite[42].

After manually locating the recorded RFs, their aggregate minimum response field was quantitatively determined using a sparse noise stimulus (500ms, 0.0625–0.25 deg^2 square, luminance decrement, 5-15 trials) and all subsequent stimuli were centered on this field. Orientation, eye, spatial and temporal frequency preferences for the cells in the recorded V1 column were determined using 1º diameter, 100% contrast drifting gratings monocularly presented on an unmodulated gray background of 45cd m^{-2} mean luminance. Inactivation experiments were run using optimal stimulus parameters. To monitor eye movements, the receptive fields were remapped by hand approximately every 10 minutes, and stimuli were re-centered in the RF when necessary. Stimuli were presented for 500ms with 750ms inter-stimulus interval. Stimuli were programmed with Matlab (Mathworks, Natick, MA) and presented on a linearized CRT monitor (Sony GDM-C520, 600 x 800 pixels, 100Hz, 57cm viewing distance) and their timing was controlled with the ViSaGe system (Cambridge Research Systems, Cambridge, UK). Data analysis was performed using custom scripts written in Matlab and Python[44,45].

Neuronal Sample Selection

We analyzed 66 visually responsive (defined as max response at least 2SD>baseline) and stimulus modulated (one-way ANOVA, $p<0.05$) units. Approximately 61% (40/66) of the visually driven single-units were modulated by one or more laser stimulation intensities (two-way ANOVA, either laser or stimulus diameter x laser interaction, $p<0.05$, or at least two successive data points different in the same direction, $p<0.05$). We were not able to determine RF size for eight cells, thus they were excluded from further analysis. For the analysis of the data presented in **figure 2**, the laser stimulation intensity producing the largest change in RF size (but within the range of intensities selected on the basis of control experiments- see **Extended Data Figs. 1-2** and Supplementary Information) was determined for each unit separately, and the analysis was performed at this intensity. For the analysis of the data presented in **figure 3,** a unit was defined as generally suppressed if the response with laser stimulation was lower than without the laser for a majority of stimulus sizes. For most units, the response with the laser on was lower than with the laser off at all stimulus sizes.

Identification of Laminar Borders

To ensure that the array was positioned orthogonal to the cortical surface, we used as criteria the vertical alignment of the mapped RF at each contact, and the similarity in the orientation tuning curves recorded at each contact (see **Extended Data Fig. 3**). The array was removed from cortex and repositioned, if significant RF misalignments across contacts were detected. The borders between the granular layer (4C) and supra- and infragranular layers were determined by applying current source density (CSD) analysis, using the kernel CSD method[46], to the band-pass filtered (1-100 Hz) and trial averaged (n=400) continuous voltage traces evoked by a brief full-field luminance increment (100ms, every 400ms, 1-89cd m^{-2}). As previously established[47], the first current sink corresponds to the granular layer, and its borders with the supra- and infra-granular layers can be determined from the reversals from sink to source above and below the granular layer, respectively.

Laser Stimulation

A 532nm laser (Laserwave, Beijing, China) beam was coupled to a 400µm diameter (NA=0.15) optical fiber, then expanded and collimated to a 2.8 mm spot. Reported irradiances refer to the light power exiting the collimator divided by the area of the collimator. Because the beam was collimated, the illumination spot size depended very little on the distance of the fiber from the brain. Laser timing was controlled at submillisecond precision, using custom made programs running on real-time Linux. Light was shone on the surface of V1 through thinned skull in the regions of GFP expression, and V2 was shielded from light. Laser onset was simultaneous with stimulus onset and photostimulation continued throughout stimulus presentation (500ms). The animal's eyes were shielded from the laser light.

Statistical Analysis

Statistical p-values refer to either independent sample or one sample two-tailed t-tests. For the within layer comparisons (**Fig.2b$_4$**) where the expected effect direction was known, one-tailed t-tests are reported. The p-value for the laminar distribution of generally suppressing cells (**Fig.3f**) ($p_{bootstrap}$, see main text) was computed by randomly sampling layer labels from a uniform distribution, and computing the proportion of samples in which the proportion exceeded that observed experimentally.

Suppression Index

The Suppression Index (SI) in **Fig. 2c$_{2\text{-}3}$** was computed as follows: $SI_{no\text{-}laser} = (R_{C\text{-}no\text{-}laser} - R_{CS\text{-}no\text{-}laser})/ R_{C\text{-}no\text{-}laser}$. $SI_{laser} = (R_{C\text{-}no\text{-}laser} - R_{CS\text{-}laser})/ R_{C\text{-}no\text{-}laser}$, where $R_{C\text{-}no\text{-}laser}$ is the response to a stimulus confined to the RF (the peak of the summation curve) in the no-laser condition, $R_{CS\text{-}no\text{-}laser}$ is the response to the stimulus covering the RF and surround in the no-laser condition (the proximal surround only for the measurements in **Fig. 2c$_2$**, and the full extent of the surround for the measurements in **Fig. 2c$_3$**), and $R_{CS\text{-}laser}$ is the response to the stimulus covering the RF and surround in the laser condition.

Histology

On completion of the recording session, the animal was perfused transcardially with 2-4% paraformaldehyde in 0.1M phosphate buffer. The occipital pole was frozen-sectioned at 40µm, tangentially to the cortical surface (n=2 brains), or sagittally (n=1). GFP label in V2 and V1 and DiI tracks were visualized under fluorescence to ascertain injection sites were confined to V2, and electrode penetrations were targeted to regions expressing GFP (**Fig.1c-d**). Electrode

442 penetrations from regions with low GFP expression were eliminated from analysis. Sections
443 were counterstained with DAPI (Sigma-Aldrich, St. Louis, MO) to identify V1/V2 border and
444 cortical layers (**Fig.1c**).

445 **REFERENCES (numbering to continue from references in the main text)**

446 41 Federer, F. *et al.* Four projections streams from primate V1 to the cytochrome oxidase
447 stripes of V2. *J. Neurosci.* **29**, 15455-15471 (2009).
448 42 Rossant, C. *et al.* Spike sorting for large, dense electrode arrays. *Nat. Neurosci.* **19**, 634-
449 641 (2016).
450 43 Kadir, S. N., Goodman, D. F. & Harris, K. D. High-dimensional cluster analysis with the
451 masked EM algorithm. *Neural. Comput.* **26**, 2379-2394 (2014).
452 44 Hunter, J. D. Matplotlib: A 2D graphics environment. *Comput. Sci. Eng*, **9**, 90-95 (2007).
453 45 van der Walt, S., Colbert, S. C. & Varoquaux, G. The NumPy Array: A Structure for
454 Efficient Numerical Computation. *Comput. Sci. Eng.* **13**, 22-30 (2011).
455 46 Potworowski, J., Jakuczun, W., Leski, S. & Wojcik, D. Kernel current source density
456 method. *Neural. Comput.* **24**, 541-575 (2012).
457 47 Schroeder, C. E., Mehta, A. D. & Givre, S. J. A spatiotemporal profile of visual system
458 activation revealed by current source density analysis in the awake macaque. *Cerebral*
459 *Cortex* **8**, 575-592 (1998).
460

SUPPLEMENTARY INFORMATION

Analysis of Surround Field Size

For the population of cells showing an increase in RF diameter when feedback was inactivated, we found no changes in the size of the surround field. Average surround diameter in the no-laser vs. laser condition was 4.71±0.43º vs. 5.38±2.77º (p=0.33). At high laser intensity, many cells showed general response suppression for small and large stimuli. These cells also showed an increase in RF size (see main text), but no significant increase in the size of the suppressive surround fields (mean surround diameter in the no-laser vs. laser condition: 4.48±0.43º vs. 4.07±0.53º, p=0.57).

Control Experiments in Cortex Not Expressing ArchT

For the main experiment, laser intensities were selected based on a control experiment in one animal (n=2 penetrations) on cortex not expressing ArchT. Recordings and analysis were otherwise identical to the main experiment.

We found light artifacts at relatively low light intensities (63mW/mm^2; see **Extended Data Fig.1a**), which, to our surprise, have been commonly used in previous optogenetic experiments. The laser artifacts were qualitatively different in superficial and deep layers: spike-rates were usually increased in superficial layers, but decreased in deep layers (**Extended Data Fig.1a)**. For granular and infragranular layers, irradiances at or below 43mW/mm^2 did not produce statistically significant changes in the cells' size tuning curves (e.g. **Extended Data Fig.1a**). For some contacts (8/16) in supragranular layers, instead, the laser-on and control curves differed significantly at 43mW/mm^2 irradiance. Importantly, however, the effect of light on these cells was always a *decrease* in RF diameter, i.e. an effect opposite to that caused by the laser in ArchT expressing cortex (**Extended Data Fig.1a)**. Because these light artifacts could not account for the observed effects of feedback inactivation, we included in our main analysis laser intensities up to 43mW/mm^2.

However, to further corroborate that our results of feedback inactivation could not be attributed to laser-induced artifacts, we repeated all the main analyses of data recorded in ArchT-expressing cortex, after excluding supragranular units which showed inactivation effects at laser irradiances >19mW/mm^2, i.e. irradiance levels that may produce artifacts in supragranular layer cells. The results of this analysis were qualitatively and quantitatively similar to the original analysis. Importantly, we performed a similar analysis for the population of units recorded in cortex not expressing ArchT, including supragranular cells at laser irradiance of 19mW/mm^2, and granular and infragranular cells at laser irradiance of 43mW/mm^2; we found not statistically significant changes in RF diameter or response amplitude in the proximal surround in the control data at these laser intensities. The results of these analysis are described below.

Analysis of Control Data in Cortex Not Expressing ArchT ***(Extended Data Fig.1)****.*
We included in this analysis supragranular cells at laser irradiance of 19mW/mm^2, and infragranular cells at laser irradiance of 43mW/mm^2 (n=10 reliable contacts). Laser illumination induced no significant changes in RF diameter (mean±s.e.m no-laser vs. laser: 1.8±0.06º vs.

1.7±0.12º, p=0.66; mean decrease 6.61±4.72%; **Extended Data Fig.1b**) or response amplitude in the proximal surround (no-laser vs. laser: 113.6±15.43 vs. 111.5±15.81, p=0.74; mean decrease 8.3±3.10%; **Extended Data Fig.1c**). This demonstrates that the effects on V1 cells' RF size and surround suppression that we observed after inactivating V2 feedback did not reflect artifacts produced by light.

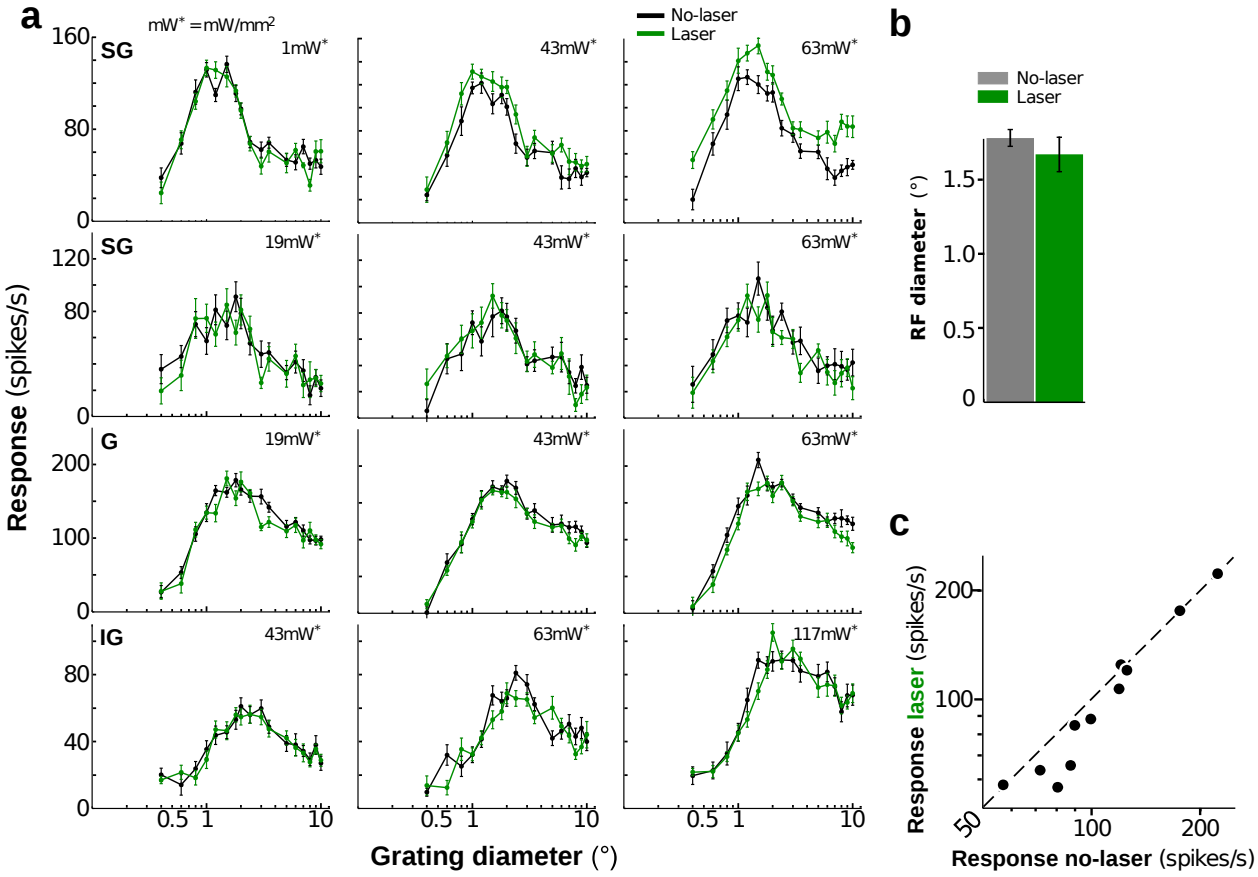

Extended Data Figure 1

Extended Data Figure 1. Light intensity selection for the main experiments. (a) Spatial summation curves in control cortex not expressing ArchT for four example units in different layers recorded at different light intensities. **(b)** RF sizes measured without (grey) and with (green) laser stimulation. The RF sizes were not significantly different. **(c)** Responses (n=11) at the proximal surround were not significantly different without and with laser stimulation.

*Analysis of Data in Cortex Expressing ArchT, excluding supragranular cells showing inactivation effects at >19mW/mm² irradiance (**Extended Data Fig.2**).*

Mean RF diameter was significantly smaller with intact feedback, compared to when feedback was inactivated (mean±s.e.m no-laser vs. laser: 1.24±0.11º vs. 1.83±0.17º, p=0.007; **Extended Data Fig.2a**), with a mean increase of 59.3±13.0% (p<0.001). As for the original analysis (**Fig. 2c**), stimuli extending into the proximal surround evoked larger neuronal responses (no-laser vs. laser: 42.0±15.4 vs. 51.8±21.5 spikes/s; mean increase 30.0±6.34%, p<0.01; **Extended Data Fig.2b$_1$**), and, therefore, less surround suppression when feedback was inactivated compared to when feedback was intact. Laser stimulation reduced the suppression index (SI) for stimuli

covering the RF and proximal surround (SI no-laser vs. laser: 0.18±0.03 vs. -0.02±0.06, p<0.01; **Extended Data Fig.2b$_2$**). In contrast, the response (no-laser vs. laser: 13.1±2.63 vs. 13.3 ±2.73 spikes/s; mean spike-rate increase 10.6±11.2%, p=0.37) and SI (no-laser vs. laser: 0.57±0.05 vs. 0.55±0.06; **Extended Data Fig.2b$_3$**) evoked by stimuli extending into the more distal surround were unchanged by feedback inactivation. Stimuli confined to the neurons' RF evoked lower responses in the laser condition (41.1±19.2 spikes/s) vs. the non-laser condition (50.1±17.6 spikes/s; mean reduction 30.3±6.34%, p<0.001; **Extended Data Fig.2c**). We conclude that increased RF diameter and reduced surround suppression indeed resulted from inactivating V2 feedback to V1, and were not caused by laser-induced heat artifacts.

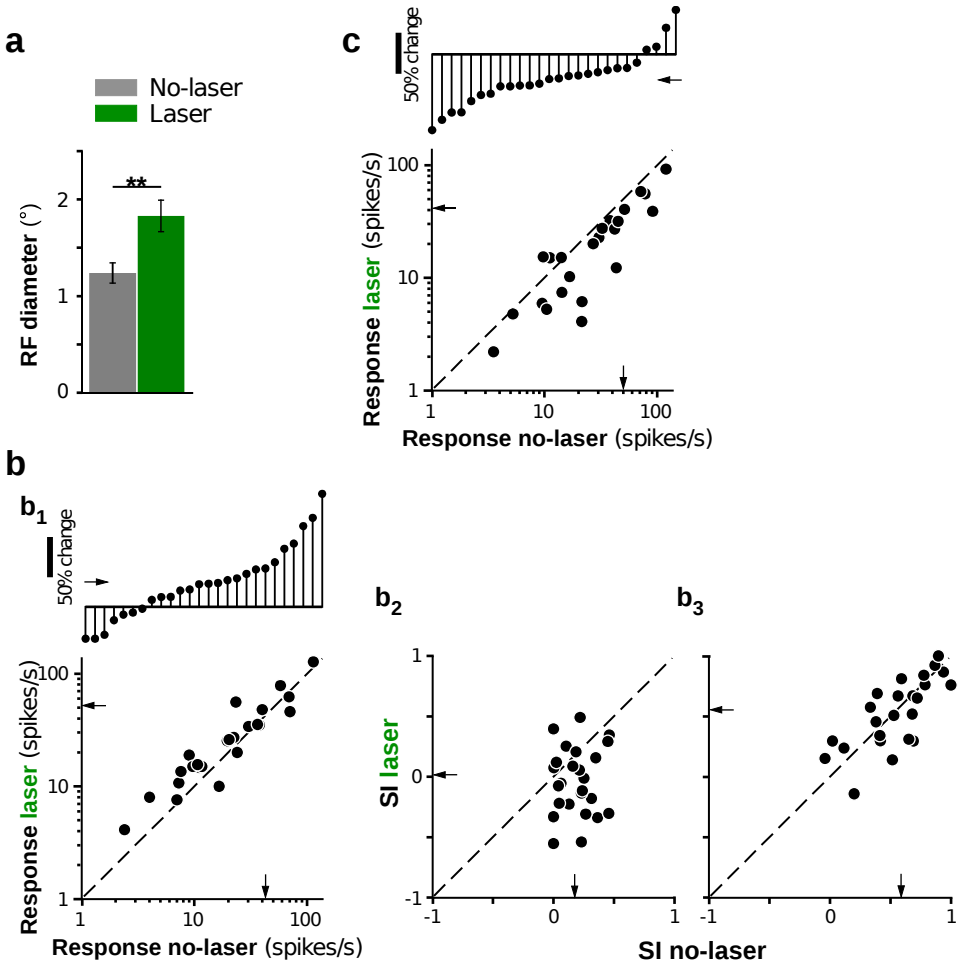

Extended Data Figure 2

Extended Data Figure 2. Analysis in cortex expressing ArchT, excluding supragranular cells showing light-induced artifacts at laser irradiance >19 mW/mm2. (a) Mean RF diameter with and without laser stimulation. (b) Changes in surround suppression with V2 feedback inactivated. (b1) BOTTOM: response with and without laser for stimuli involving the RF and proximal surround. TOP: Cell-by-cell percent response change caused by laser stimulation, for stimuli extending into the proximal surround. (b2) SI with and without laser for stimuli extending into the proximal surround. (b3) Same as (b2) but for stimuli extending into the distal surround. (c) BOTTOM: response with and without laser for stimuli confined to the RF. TOP: Cell-by-cell percent response change caused by laser stimulation, for stimuli confined to the RF.

None of the units recorded in the control experiment showed reduced response at the irradiances used for the analysis of data in **Fig.3**. Thus, we are confident that the general response suppression for small and large stimuli observed in the data reported in **Fig.3**, resulted from inactivating feedback axons.

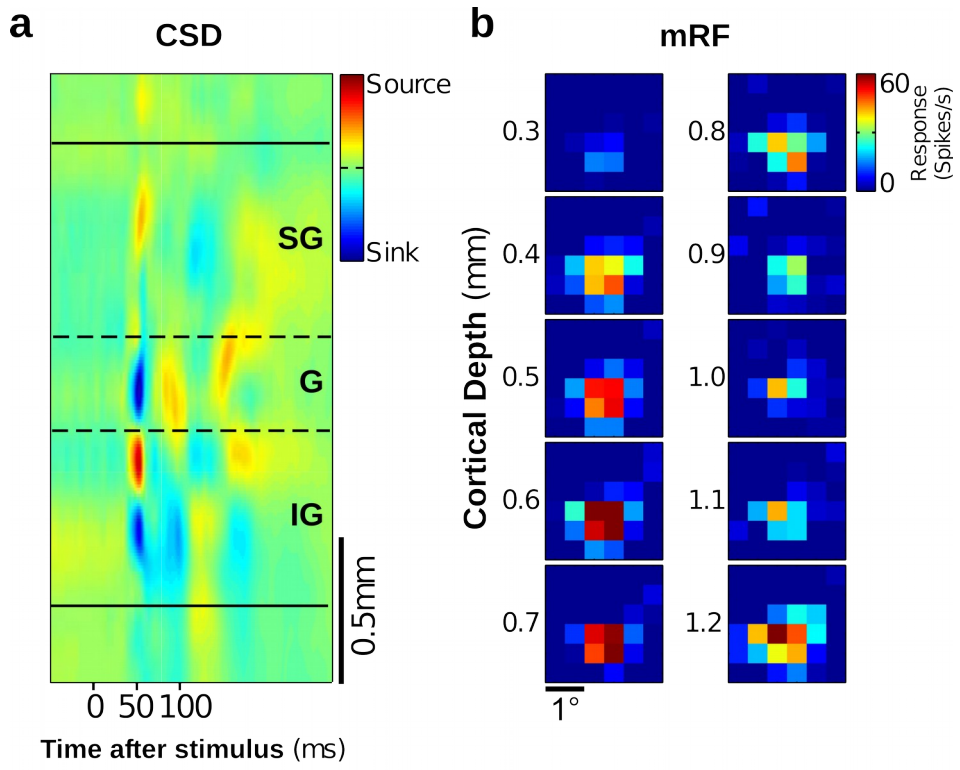

Extended Data Figure 3

Extended Data Figure 3. Recordings of CSD and minimum RF (mRF) ensure linear array spans all cortical layers, and is positioned normal to cortical surface. (a) Current source density (CSD) analysis of local field potential (LFP), used to determine cortical layers and ensure contacts span the full extent of the cortical sheet. (b) mRF mapping (see Methods) across contacts through the depth of V1. Hot spots (regions of max spiking rate) are aligned across contacts, confirming the array is positioned normal to the V1 surface. SG: Supragranular layers, G: Granular layer, IG: Infragranular layers.

Control Analysis for Laser Stimulation Time

Inactivation of axon terminals using ArchT can, counter intuitively, facilitate synaptic transmission for prolonged light pulses, while ArchT is consistently suppressive for pulse widths of ≤ 200ms. Thus, we repeated our analysis by focusing only on the first 200ms of the response. We found no qualitative differences between the original analysis and the short time-scale analysis. Consistent with the original analysis, RF diameter was increased when feedback was inactivated (no-laser vs. laser: 1.14±0.07º vs. 1.67±0.24, $p<0.05$, n=19 units producing reliable responses within the initial 200ms), responses to stimuli confined to the RF were significantly reduced (no-laser vs. laser: 26.1±8.89 vs. 21.6±10.3 spikes/s; mean spike-rate reduction 45.1±8.62%, $p<0.001$), and responses to stimuli covering the RF and proximal surround were

551 increased (mean spike-rate increase 67.6±34.0 %, $p<0.06$). We conclude that the observed laser-
552 induced effects reflect suppressed, rather than facilitated, V2 feedback activity.